Materials Today Communications xxx (xxxx) 108415

Contents lists available at ScienceDirect

Materials Today Communications

journal homepage: www.elsevier.com/locate/mtcomm

Connecting dielectric response to dominant vibrations and tolerance factors in pyrochlore oxides

Sonu Kumar [a, b, *], Karandeep [c], Shagun Nag [d], Ranjan Kumar [e]

[a] Department of Physics & Astronomical Science, Central University of Himachal Pradesh, Temporary Academic Block, Shahpur, Kangra 176206, India
[b] Institute for Chemical Reaction Design and Discovery (WPI-ICReDD), Hokkaido University, Sapporo 001-0021, Japan
[c] Lajpat Rai D.A.V. College, Jagraon, Punjab 142026, India
[d] Department of Physics, Government College, Dhaliara, Kangra, Himachal Pradesh 177103, India
[e] Department of Physics, Panjab University, Chandigarh 160014, India

ARTICLE INFO

Keywords:
Pyrochlores
Dielectric screening
Density functional theory
Infrared vibrations
Phonons

ABSTRACT

Dielectric screening originating from electronic and vibrational degrees of freedom is a fundamental material's property. This property is crucial for materials used as high K-gate dielectric with metal gates in field-effect transistors in integrated circuits. Therefore, we atomically explore phonons responsible for dielectric screening in rare-earth pyrochlores zirconate oxides, $RE_2Zr_2O_6O'$ (RE = Pr, Nd, Sm, Eu, and Gd), and suggest pathways for engineering the dielectric response for better dielectric insulators. The predicted crystal structures are close to the ideal pyrochlore structure but show a tendency towards the fluorite structure along the family (which alters dielectric screening). A significant contribution towards the dielectric screening originates from the infrared-active vibration (F_{1u} named as m_2) near 125 cm^{-1}, which is mainly due to O'-RE-O' bend. The vibration near 200 cm^{-1} also has notable contribution but shows a gradual decrease along the family. A relation between tolerance factors (t_1 and t_2) of pyrochlores and dielectric response is developed for the first time. Specifically, a linear relation of t_2 with dominating vibration (m_2) contributing to the dielectric constant paves the way to engineer the dielectric screening by a simple calculation of the tolerance factor in pyrochlore zirconates.

1. Introduction

Pyrochlore oxides have been studied over decades owing to their numerous technological important applications like dielectrics [1–5], superconductivity [6], thermal barrier coating [7], gas sensing [8], luminescence [9], and chemical durability [10]. All zirconate pyrochlores are found to exhibit radiation resistance except $La_2Zr_2O_7$ [11]. $Gd_2Zr_2O_7$ shows high radiation resistance and is proposed to be the host material for the immobilization of plutonium and actinides [12]. Different pyrochlore oxides show electrical properties [13], high entropy [14] and catalytic properties [15], and ferroelectricity [16]. Also, pyrochlore oxides find their applications in high ceramic dielectric materials [17] such as $La_2Zr_2O_7$ [18] and $La_2Hf_2O_7$ [19]. Rare-earth titanate pyrochlores exhibit interesting magnetic properties like spin ice and spin glass behaviors due to their characteristic crystal structure and magnetic interactions [20].

In ideal pyrochlores of the type $A_2B_2O_6O'$, A type cation is a rare-earth (RE) lanthanide or a cation with lone pair of electrons; B type cation is a transition-metal with variable oxidation state or a post transition metal cation; O and O' are oxygen atoms with different atomic environments. The tetrahedral environment around O and O' atoms is shown in Figs. 1(a) and 1(b), respectively. When A and B type atoms are in 3^+ and 4^+ ionized state, or 2^+ and 5^+ states, respectively, then these oxides are referred to as ($3+$, $4+$) or ($2+$,$5+$) type pyrochlores [21]. Average mixed valency of these types in also possible. Eight-units of $A_2B_2O_7$ or $A_2B_2O_6O'$ (Here A = RE, B = Zr) comprise the conventional unit cell of pyrochlore structure.

An increased interest in these oxides is consequence of A and B type elements residing on the two interpenetrating lattices of the corner-sharing tetrahedron. Raman and Infrared vibrations in these oxides provide a beautiful insight into various dynamical processes involving phonons, charge carriers, and spin affecting physical and chemical properties. Information about the distribution of ions at different symmetry sites, deviation from site symmetry induced either by point defects or local stress is also possible. Vibrational properties in pyrochlore oxides have been the subject of extensive experimental investigations

* Corresponding author at: Department of Physics & Astronomical Science, Central University of Himachal Pradesh, Temporary Academic Block, Shahpur, Kangra 176206, India.
E-mail address: sonukumar.physics@gmail.com (S. Kumar).

https://doi.org/10.1016/j.mtcomm.2024.108415
Received 30 December 2023; Received in revised form 30 January 2024; Accepted 16 February 2024
2352-4928/

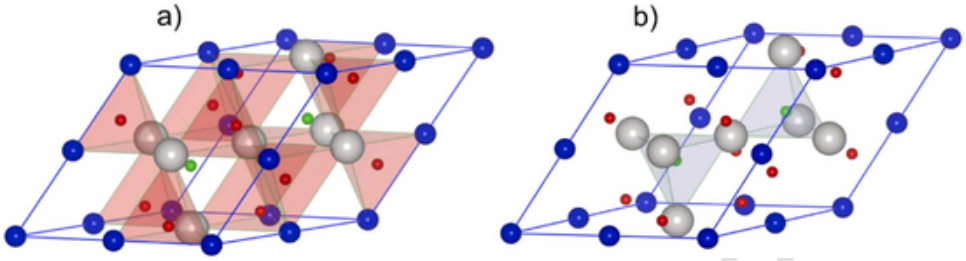

Fig. 1. Primitive unit cell showing the a) tetrahedral environment around O atom, and b) tetrahedral environment around O' atoms in $RE_2Zr_2O_7$ (RE = Pr, Nd, Sm, Eu and Gd) pyrochlore zirconate oxides. Color code: RE: Gray, Zr: blue, O: red, and O': green.

[22,23] as well as theoretical investigations [24–26]. Further, information about the strength of bonding and its effect on vibrational properties can provide atomic-level information of tailoring the macroscopic properties like the static dielectric constant in these materials.

Dielectric screening is a fundamental property in materials and has its origin from the intrinsic and extrinsic response to the external electric field. The intrinsic response to the dielectric constant comes from (1) the electronic degrees of freedom (electrons screening with clamped ions to the applied electric field), and (2) the lattice degrees of freedom (screening due to motion of ions in response to the electric field) [27]. Whereas extrinsic response comes from defects (point and line defects), ferroelectric domains, surfaces and edges (in low dimensional materials), and interfaces [28]. These extrinsic factors affect the intrinsic response, and therefore, the dielectric response can be altered significantly [28]. Dielectric properties are quite important as scaling down of random-access memories (static as well dynamic) based on capacitive functionality can be achieved using materials with high dielectric constant compared to the already used materials such as SiO_2. Similarly, low dielectric constant materials are vital for high-speed interconnects in integrated circuitry. The dielectric constant originating from dielectric screening affects the electronic bandgap as well as the binding energies. Recently, dielectric screening is found to display a significant role in reduced dimensional materials due to decreased dielectric constant in the out-of-plane direction [29], indicating the usefulness of dielectric screening. Therefore, exploration of the intrinsic response is crucial for understanding the dielectric behavior in oxides, leading to the study of zirconate pyrochlores in the present study as an example. Previous studies explored dielectric properties of hafnate [30] and titanate [31] pyrochlores.

Further, the tolerance factor concept (given by Goldschmidt for perovskites [32]) is beneficial not only to study the structural stability of oxides but also provides a significant information about the physical properties [33]. In this vein, we explore, for the first time, the tolerance factors (given by Cai et al. [34] for pyrochlores) for their relations with structural as well as dielectric behavior. To explore the influence of A type atom in these oxides on dielectric environment, we study vibrations contributing to dielectric properties of $RE_2Zr_2O_7$ (RE = Pr, Nd, Sm, Eu and Gd) using density functional theory (DFT) [35] based on plane wave basis and ultrasoft pseudopotentials (USPPs) [36]. Changing the electronic and ionic environment by replacing A-type atoms will lead to a systematic response and explanation to dielectric screening. Afterward, a relation of dielectric constant with tolerance factors is investigated. The paper is organized as follows. In Sec. II, the computational method is introduced in detail. In section III, we will give results and discussions. In Sec. IV, we will conclude our results and their importance.

2. Computational details

Energy and phonon calculations are carried out using density functional theory based on Quantum Espresso package [37]. The exchange and correlation interactions are described within local density approximation (LDA [38,39]) and generalized gradient approximation (GGA [40]), specifically PBEsol [41]. The LDA is found to provides a good description of the structural [42], vibrational and dielectric properties of pyrochlore oxides [24,25], whereas PBEsol functional has better structural properties descriptions for solids. Our key findings are similar for both functionals. A detailed structural parameter of these pyrochlores is provided in the supplementary information (Figure S1, Figure S2, Table S1, and Table S2). The DFT results correspond to a temperature of 0 K.

USPPs for the Pr, Nd, Sm, Eu, and Gd atoms in their 3+ state with the f-states in the core are generated. The effect of f-states is taken through the non-linear core-correction. These potentials, although hard, are tested on pyrochlores [25] and perovskites [43] and are transferable along with potential of oxygen [44].

All the input files are generated using EStA [45]. We used a plane wave cutoff of 90 Ry and a charge density cutoff of atleast ten times that of plane wave cutoff to guarantee a pressure tolerance of less than 1 kbar. A dual space grid technique is used to calculate the charge density and the self-consistent potential. Broyden-Fletcher-Goldfarb-Shanno (BFGS) algorithm [46] is used to search for the minimum energy configuration. For the equilibrium structures, force tolerance is less than 0.4 meV/Å per atom in each Cartesian direction. Kohn-Sham one-particle equations are solved at each k point in reciprocal space using a $3\times3\times3$ k Monkhorst-Pack grid [47]. Phonon frequencies are calculated using density functional perturbation theory and phonopy [48,49]. The dielectric constants contribution from individual modes (explained in results and discussion) are computed using the inhouse program.

3. Results and discussions

3.1. Developing relationship between lattice vibrations and dielectric response

Vibrations in materials, specifically infrared active phonons, are intrinsically related to dielectric screening. To find the nature of vibrational modes in cubic rare-earth pyrochlore structure ($RE_2Zr_2O_6O'$), we use correlation and factor group analysis [50]. This analysis gives the following irreducible representations (irreps) for the different sublattices in the pyrochlore unit cell at the gamma point:

$$\begin{aligned}\text{RE sublattice} &= A_{2u} + E_u + 2F_{1u} + F_{2u};\ \text{Zr sublattice}\\ &= A_{2u} + E_u + 2F_{1u} + F_{2u}\\ \text{O sublattice} &= A_{1g} + E_g + 2F_{1g} + 3F_{2g} + A_{2u}\\ &\quad + E_u + 3F_{1u} + 2F_{2u};\ O'\text{sublattice}\\ &= F_{1u} + F_{2g}\end{aligned}$$

Thus, the total irreducible representation (excluding acoustical modes):

$$\Gamma_{vib}^{crys} = A_{1g} + E_g + 2F_{1g} + 4F_{2g} + 3A_{2u} + 3E_u + 7F_{1u} + 4F_{2u} \quad (1)$$

There are seven infrared (IR) active modes ($7F_{1u}$) and six Raman active modes (A_{1g}, E_g, $4F_{2g}$). Remaining modes are optically inactive. The infrared active vibrations are shown in the Fig. 2. The Raman phonon modes along with symmetry are provided in the supplementary information in Figure S3 and Table S3.

Lattice vibrations contribute to the dielectric screening. More is the screening, the higher the static dielectric constant. The static dielectric constant is a sum of the electronic and the ionic parts, i.e., $\vec{\vec{\varepsilon}}_o = \vec{\vec{\varepsilon}}_{elec} + \vec{\vec{\varepsilon}}_{ion}$.The ionic part contains the contribution from the infrared-active phonons and the Born effective charges. This part is usually dominant than the electronic part in high-k insulators. We implement and compute the static dielectric constant and the mode-oscillator strength of individual vibrational modes using the following approach [27]:

$$\varepsilon^{0}_{\alpha\beta} = \varepsilon^{\infty}_{\alpha\beta} + \varepsilon_{ion} = \varepsilon^{\infty}_{\alpha\beta} + \sum_{m} \Delta\varepsilon_{m,\alpha\beta} \tag{2}$$

Where m labels the zone center (q = 0) infrared-active vibrations. The electronic part is given by

$$\varepsilon^{\infty}_{\alpha\beta} = \delta_{\alpha\beta} + 4\pi \left.\frac{\partial P_{\alpha}}{\partial \epsilon_{\beta}}\right|_{\zeta=0} \tag{3}$$

with polarization P induced by the electric field ϵ with the condition that all the ions are fixed at their positions, $\zeta = 0$.The ionic contribution is:

$$\sum_{m} \Delta\varepsilon_{m,\alpha\beta} = \frac{4\pi e^2}{\Omega} \sum_{m} \frac{S_{m,\alpha\beta}}{\omega^2_m} \tag{4}$$

with mode-oscillator strength tensor given by

$$S_{m,\alpha\beta} = \left(\sum_{k\alpha'} Z^{*}_{k,\alpha\alpha'} u^{*}_{m}(k\alpha')\right)\left(\sum_{k'\beta'} Z^{*}_{k',\beta\beta'} u_{m}(k'\beta')\right) \tag{5}$$

$u_m(k\alpha)$ refers to the eigen displacement of the k^{th} atom along α direction in m^{th} mode and Ω is the volume of the unit cell. $Z^{*}_{k,\alpha\beta}$ is the dynamical charge or Born effective charge and is defined in terms of change in total polarization (ionic + electronic) when an atom is displaced from its equilibrium position. Mathematically, the Born-effective charge matrix element for the k^{th} atom is defined by:$Z^{*}_{k,\alpha\beta} = \frac{\Omega}{e}\frac{\partial P_{\beta}}{\partial \tau_{k,\alpha}}$; where P_{β} is the β component of the macroscopic polarization induced per unit cell, when the k^{th} atom is displaced along the direction given by the index α. Further, to fulfill the charge neutrality, the sum of the Born effective charges of all atoms in the unit cell has to be zero i.e., $\sum_k Z^{*}_{k,\alpha\beta} = 0$.The components of mode effective charge of the m^{th} mode, Z^{*}_{m} can be calculated (once we know the Born-effective charges and the eigen-displacements of all the modes) as follows [27]:

$$Z^{*}_{m,\alpha} = \frac{\sum_{k\beta} Z^{*}_{k,\alpha\beta} u_{m,\mathbf{q=0}}(k\beta)}{\left[\sum_{k\beta} u^{*}_{m,\mathbf{q=0}}(k\beta)\ u_{m,\mathbf{q=0}}(k\beta)\right]^{1/2}} \tag{6}$$

The Born charges arise due to dynamical changes in hybridization during the vibrations of atoms. The calculated Born effective charges for pyrochlore zirconates are given in Table 1. The rare-earths and the Zr atom occupy positions with D_{3d} point group symmetry, resulting in two different values of Born effective charges: one due to the displacement in [111] direction and other degenerate values in the orthogonal direction. The Born effective charges associated with the O atom (having C_{2v} point group) are all non-degenerate, indicating anisotropy in different directions. In contrast O' atom's charges (present at the site of T_d point symmetry) are triply degenerate and isotropic. It may be noted that the O atom is surrounded by two Zr atoms and two rare-earth atoms in a tetrahedral fashion, whereas O' atom is surrounded by four rare-earth in a tetrahedral environment indicating the difference in the local environment around the O and O' atoms. This different environment manifests itself in the Born-effective charges during the vibrational motion of the atoms. Further, the Born effective charges for RE, Zr, O, and O' atoms at 16c, 16d, 48 f, and 8b sites deviate from their nominal charges +3e, +4e, −2e, and −2e, respectively, indicating their anomalous values. Along the zirconate pyrochlore family, we observed a small change in the Born-effective charges associated with the atoms indicating minor dynamical changes in hybridization during the vibrations.

In pyrochlore oxides, there are seven infrared active F_{1u} vibrations. Generally, in pyrochlores, these vibrations span frequency range from around 70–600 cm^{-1} [21,24] except the stannate and platinate pyrochlores with frequencies exceeding 600 cm^{-1}. Table 2 shows DFT calculated infrared-active vibrations along with the experiments. Our calculations find the lowest frequency mode i.e., the first mode, m_1, near 90 cm^{-1} and the second mode, m_2, near 125 cm^{-1}. Modes m_1 and m_2 were attributed to O'-RE-O' bend and O-RE-O bend respectively by McCauley [51]. Similarly, the remaining polar modes were assigned as follows: the mode m_3 (near 190 cm^{-1}) to RE-ZrO_6 stretch, the mode m_4 (near 205 cm^{-1}) to O-Zr-O bend, the mode m_5 (near 340 cm^{-1}) to RE-O stretch, the mode m_6 (near 400 cm^{-1}) to RE-O' stretch, and the mode m_7 (near 515 cm^{-1}) to the Zr-O stretch. Along the pyrochlore family, an

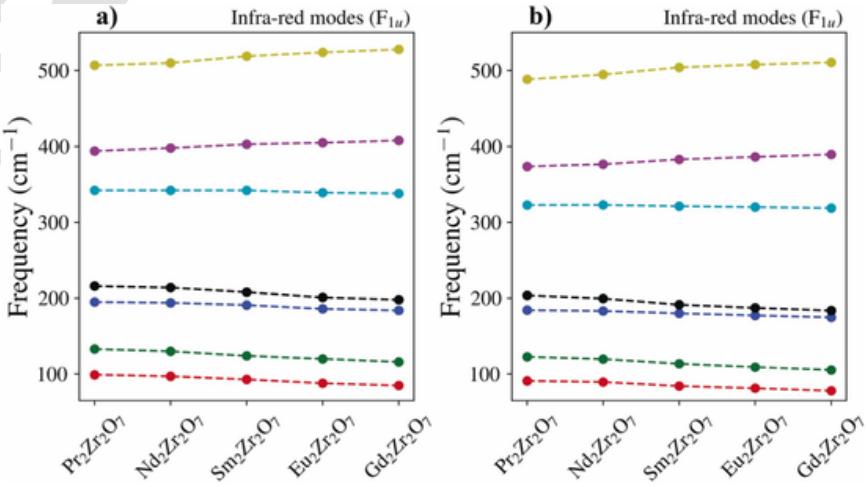

Fig. 2. Variation of Infrared active vibrational modes in pyrochlore zirconates, $RE_2Zr_2O_7$ (RE= Pr, Nd, Sm, Eu and Gd) using a) LDA, and b) PBEsol functionals.

Table 1
DFT calculated Born effective charges with RE ion centered at (1/2, 1/2, 1/2), Zr ion at (0, 0, 0), O_{48f} ion at (x, 1/8, 1/8) and O_{8b} ion at (3/8, 3/8, 3/8) for pyrochlore zirconates. Eigenvalues obtained after diagonalizing the Born effective charge matrices are also given in square brackets.

material	Z^*_{RE}	Z^*_{Zr}	$Z^*_{O_{48f}}$	$Z^*_{O_{8b}}$
$Pr_2Zr_2O_7$	$\begin{pmatrix} 4.094 & -0.096 & -0.096 \\ -0.096 & 4.094 & 0.096 \\ -0.096 & 0.096 & 4.094 \end{pmatrix}$	$\begin{pmatrix} 5.714 & 0.378 & 0.378 \\ 0.378 & 5.714 & -0.378 \\ 0.378 & -0.378 & 5.714 \end{pmatrix}$	$\begin{pmatrix} -2.963 & 0.0 & 1.016 \\ 0.0 & -2.493 & 0.0 \\ 1.016 & 0.0 & -2.963 \end{pmatrix}$	-2.794
	[4.286, 3.998, 3.998]	[6.092, 6.092, 4.958]	[−1.947, - 2.493, −3.979]	
$Nd_2Zr_2O_7$	$\begin{pmatrix} 4.078 & -0.081 & -0.081 \\ -0.081 & 4.078 & 0.081 \\ -0.081 & 0.081 & 4.078 \end{pmatrix}$	$\begin{pmatrix} 5.713 & 0.38 & 0.38 \\ 0.38 & 5.713 & -0.38 \\ 0.38 & -0.38 & 5.713 \end{pmatrix}$	$\begin{pmatrix} -2.958 & 0.0 & 1.016 \\ 0.0 & -2.491 & 0.0 \\ 1.016 & 0.0 & -2.958 \end{pmatrix}$	-2.777
	[4.240, 3.997, 3.997]	[6.093, 6.093, 4.953]	[−1.942, - 2.491, −3.974]	
$Sm_2Zr_2O_7$	$\begin{pmatrix} 4.047 & -0.045 & -0.045 \\ -0.045 & 4.047 & 0.045 \\ -0.045 & 0.045 & 4.047 \end{pmatrix}$	$\begin{pmatrix} 5.706 & 0.393 & 0.393 \\ 0.393 & 5.706 & -0.393 \\ 0.393 & -0.393 & 5.706 \end{pmatrix}$	$\begin{pmatrix} -2.946 & 0.0 & 1.004 \\ 0.0 & -2.496 & 0.0 \\ 1.004 & 0.0 & -2.946 \end{pmatrix}$	-2.742
	[4.137, 4.002, 4.002]	[6.099, 6.099, 4.920]	[−1.942, - 2.496, −3.950]	
$Eu_2Zr_2O_7$	$\begin{pmatrix} 4.030 & -0.028 & -0.028 \\ -0.028 & 4.030 & 0.028 \\ -0.028 & 0.028 & 4.030 \end{pmatrix}$	$\begin{pmatrix} 5.704 & 0.398 & 0.398 \\ 0.398 & 5.704 & -0.398 \\ 0.398 & -0.398 & 5.704 \end{pmatrix}$	$\begin{pmatrix} -2.94 & 0.0 & 0.999 \\ 0.0 & -2.5 & 0.0 \\ 0.999 & 0.0 & -2.94 \end{pmatrix}$	-2.724
	[4.086, 4.002, 4.002]	[6.102, 6.102, 4.908]	[−1.941, - 2.500, −3.939]	
$Gd_2Zr_2O_7$	$\begin{pmatrix} 4.015 & -0.011 & -0.011 \\ -0.011 & 4.015 & 0.011 \\ -0.011 & 0.011 & 4.015 \end{pmatrix}$	$\begin{pmatrix} 5.702 & 0.401 & 0.401 \\ 0.401 & 5.702 & -0.401 \\ 0.401 & -0.401 & 5.702 \end{pmatrix}$	$\begin{pmatrix} -2.935 & 0.0 & 0.996 \\ 0.0 & -2.497 & 0.0 \\ 0.996 & 0.0 & -2.935 \end{pmatrix}$	-2.707
	[4.037, 4.004, 4.004]	[6.103, 6.103, 4.900]	[−1.939, - 2.497, −3.931]	

Table 2
DFT calculated infrared active frequencies (cm^{-1}) of $RE_2Zr_2O_7$ (RE = Pr, Nd, Sm, Eu, Gd) pyrochlores calculated using PBEsol (LDA) approximation along with the experiments.

Infrared active	m_1	m_2	m_3	m_4	m_5	m_6	m_7
$Pr_2Zr_2O_7$							
DFT	85	121	184	200	319	376	490
	(99)	(133)	(195)	(216)	(342)	(394)	(507)
$Nd_2Zr_2O_7$							
DFT	82	117	181	195	319	378	497
	(97)	(130)	(194)	(214)	(342)	(398)	(510)
Expt. [21]	70	132	187	226	372	421	527
$Sm_2Zr_2O_7$							
DFT	77	111	177	189	319	387	506
	(93)	(124)	(191)	(208)	(342)	(403)	(519)
Expt. [21]	92	126	174	244	372	432	532
$Eu_2Zr_2O_7$							
DFT	73	107	174	185	317	389	510
	(88	(120)	(186)	(201)	(339)	(405)	(524)
Expt. [21]	-	-	170	241	350	420	530
$Gd_2Zr_2O_7$							
DFT	69	103	170	182	316	392	513
	(85)	(116)	(184)	(198)	(338)	(408)	(528)
Expt. [21]	-	-	-	218	-	462	533

increase in the frequency of mode m_5 and mode m_6 is found due to decrease in RE-O and RE-O' bond lengths.

Our DFT calculated vibrational eigen-vectors predict that the mode m_1 and m_2 should be assigned to the O-RE-O bend and the O'-RE-O' bend, respectively (as shown in Fig. 3 for mode m_2). The first four modes (m_1, m_2, m_3, and m_4) show a decrease in wave-numbers, the mode m_5 remains almost the same, and the modes m_6 and m_7 show an increase in wave-numbers along the family of pyrochlore zirconates. The decrease in the wave-numbers in modes m_1, m_2, m_3 and m_4 are mainly due to an increase in the mass of rare-earths along the family. In contrast, an increase in the wave-numbers of modes m_6 and m_7 shows the dominant contribution of respective stretching force constants which overshadows the effect of increasing mass of the rare-earths. Almost the same wave-numbers of the mode m_5 show the effect of increasing mass of rare-earth is counter-balanced by the increase in the force constant of the RE-O bond.

The mode-wise contribution of the ionic part of static dielectric constant to static dielectric constant (ε_0) and mode effective charges ($\bar{Z}^*$)are given in Table 3. The electronic part of the static dielectric constant (ε_∞) remains almost the same as we move along the zirconate family. However, there is an increase in the dielectric constant, mainly due to an increase in its ionic part.

The mode oscillator strengths ($S_{m,\alpha\beta}$) and mode effective charges ($Z^*_{m,\alpha}$) directly relate to the ionic contribution. Fig. 4 shows the mode effective charges and ionic part of static dielectric constant of all the seven infrared-active vibrations. Out of these seven F_{1u} modes, modes m_2, m_3 and m_5 have the highest mode effective charges and maximum contribution towards the static dielectric constant. Modes in the high-frequency range (m_4, m_6, and m_7) have minor mode effective charges and, therefore, smaller ionic contributions to the static dielectric constant.

The mode effective charge of mode m_1 is small despite its low frequency, resulting in a small contribution to the ionic dielectric constant. Further, moving along the pyrochlore zirconate family, a maximum increase in the ionic part of the dielectric constant due to mode, m_2, is observed. Mode m_1, m_4, and m_6 show an increase, mode m_7 remains constant, while mode m_3 and m_5 show a decrease in the ionic di-

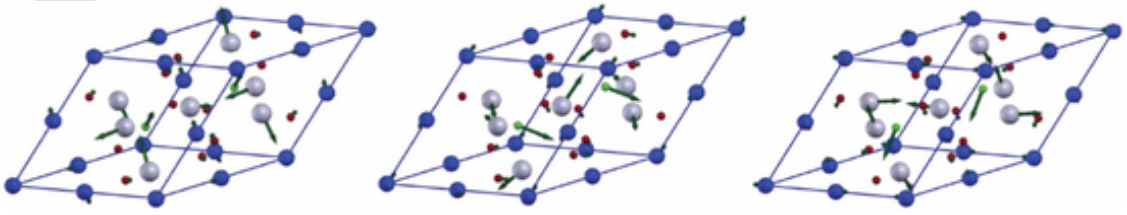

Fig. 3. Displacement pattern of atoms in infrared-active vibration, F_{1u}, represented by mode m_2 in pyrochlore zirconates. Color code: RE: gray, Zr: blue, O: red, and O': green.

Table 3
DFT calculated electronic dielectric constant (ε_∞), static dielectric constant (ε_0) and contribution of infrared active modes ($\Delta\varepsilon$) and mode effective charges ($\bar{Z}^*$) in pyrochlores (PBEsol functional).

	m_1	m_2	m_3	m_4	m_5	m_6	m_7	ε_∞	ε_0
$Pr_2Zr_2O_7$									
$\Delta\varepsilon$	1.97	10.64	9.76	0.10	7.68	0.24	0.83	4.85	36.08
$\bar{Z}^*$	2.49	7.84	8.24	0.67	12.28	1.94	4.62		
$Nd_2Zr_2O_7$									
$\Delta\varepsilon$	2.28	11.66	9.63	0.45	7.26	0.53	0.84	4.85	37.50
$\bar{Z}^*$	2.52	7.91	8.09	1.34	11.55	2.89	4.66		
$Sm_2Zr_2O_7$									
$\Delta\varepsilon$	3.57	13.03	8.98	1.72	6.77	0.82	0.84	4.84	40.57
$\bar{Z}^*$	2.84	7.78	7.45	2.58	10.78	3.66	4.68		
$Eu_2Zr_2O_7$									
$\Delta\varepsilon$	4.34	14.19	8.30	2.82	6.47	1.02	0.83	4.84	42.81
$\bar{Z}^*$	2.89	7.73	6.86	3.32	10.29	4.14	4.66		
$Gd_2Zr_2O_7$									
$\Delta\varepsilon$	4.91	15.53	7.61	3.98	6.27	1.16	0.83	4.84	45.13
$\bar{Z}^*$	2.87	7.72	6.29	3.96	9.97	4.43	4.64		

electric constant along the pyrochlore zirconate family. Overall, we observed an increase in the static dielectric constant along the family mainly due to the contribution of mode m_2. The mode m_2 is mainly due to O'-RE-O' bending as shown in Fig. 3.

3.2. Structural parameters relation to tolerance factors

Structural information, especially the local environment around cations (RE^{3+} and Zr^{3+}) is critical to influencing the dielectric response. The pyrochlores crystal lattice (with formula unit $RE_2Zr_2O_6O'$) is completely described in terms of lattice constant (a_0) and u parameter of O-atom at 48 f position (O_{48f} parameter). The point group symmetry and the coordinates of the atoms are given in the supplementary information, Table S1.

In pyrochlore crystal, RE atoms are surrounded by O and O' atoms. The oxygen atoms at 48f positions are bonded to two RE atoms and two Zr atoms, whereas the O′ atom is connected to RE atoms. The RE-O′ bond (shortest bond in these materials) depends on only a_o, and Zr-O and RE-O bonds depend upon both a_o and u parameters. Generally, the u parameter is obtained from the refinement of powder diffraction data. Since the O atom is a weaker scatter of X-rays than either of RE and Zr atoms, X-ray methods are of limited accuracy. Powder neutron diffraction methods can also give a good estimate of the u parameter, but neutron sources are not frequently available. Therefore, DFT calculated values can provide a good benchmark for the observed values of u parameters. The a_o and u parameters are given in the supplementary information Table S2. With the decrease in RE^{3+} radii (due to the lanthanide contraction) along the family of zirconates, a_0 decreases and u increases in agreement with the other pyrochlores [24]. This fact is in contradiction with calculations of R. A. McCauley [52]; in these calculation a decrease in u with a decrease in a_o is predicted. The almost linear variation of a_o with respect to RE^{3+} ion radius indicates ionicity [53].

The RE^{3+} cations located in the oxygen scalenohedral are eight coordinated (2 O' + 6 O). The Zr^{4+} ions are surrounded by the trigonal antiprism formed by the six O atoms. The RE^{3+} scalenohedron becomes a cube when u approaches 0.375 (Table S2); and Zr^{4+} trigonal antiprism becomes a perfect octahedron when u approaches 0.3125. At u = 0.3750, defect fluorite structure is obtained. This shows that the u parameter is a direct measure of the environment around Zr^{4+} cation in pyrochlore oxides. Further, u = 0.3125 corresponds to the ideal pyrochlore structure. The environment around Zr^{4+} cations is more like an octahedron, indicating that the structure in each case is close to the ideal pyrochlore structure. However, along the family pyrochlores show a tendency towards fluorite structure as indicated by the increase in the u parameter (Table S2). The bonds RE-O_{48f} and Zr-O_{48f} decrease with the decrease in the RE^{3+} ionic radii. Further, the ∠ZrOZr (∠OZrO) bond angle decreases (increases) with the decrease in a_0 along the family. For a small RE atom there is large decrease in bond lengths of ZrO_6 octahedral, which is partially compensated by the increase in the u parameter along the family (Table S2). Further, a decrease in ZrO_6 bond lengths along the family can be attributed to increase in overlap of O-2p and Zr-4d states as observed in pyrochlore oxides [25], which may significantly affect the dielectric response.

DFT calculated lattice constants are in good agreement with experimental lattice constants with a maximum relative error of ~1.4% for LDA and PBEsol functionals (see Table S2). The stability of pyrochlore type structure is determined by the radius ratio of RE (3+ state) and Zr (4+ state) cations (r_{RE}/r_{Zr}). The radius ratio with values 1.564, 1.540, 1.499, 1.481, and 1.4625 for $Pr_2Zr_2O_7$, $Nd_2Zr_2O_7$, $Sm_2Zr_2O_7$, $Eu_2Zr_2O_7$, and $Gd_2Zr_2O_7$ zirconates, respectively, are found indicating stability under ambient conditions as stability criteria $1.46 < r_{RE}/r_{Zr} < 1.78$ is fulfilled [54].

Based on the oxygen u parameter, radii of RE, Zr, and O atoms, the two tolerance factors t_1 and t_2 for pyrochlores are defined as [34]:

$$t_1 = \frac{\sqrt{(u-1/4)^2 + 1/32}}{\sqrt{(u-1/2)^2 + 1/32}} \left(\frac{r_{RE} + r_o}{r_{Zr} + r_o}\right) \tag{7}$$

and

$$t_2 = \frac{\sqrt{3}a}{8(r_{RE} + r_o)} \tag{8}$$

The r_{RE}, r_{Zr} and r_O are the ionic radii of RE, Zr and O ions in 3+, 4+, and 2- states respectively. The tolerance factor t_1 is defined with respect to the RE_2Zr_2 tetrahedra with O atom inside, and t_2 is defined with re-

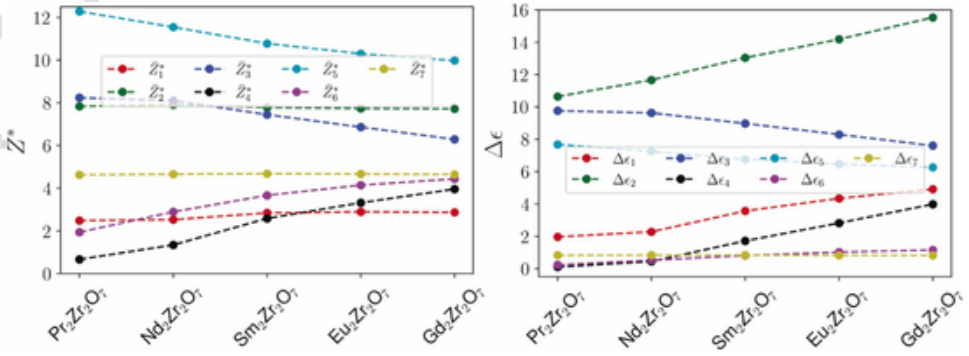

Fig. 4. Mode-effective charges of individual modes (left) and mode wise contribution of ionic dielectric constants (right) in pyrochlore zirconates using PBEsol (for LDA results, see the supplementary information Fig. S4).

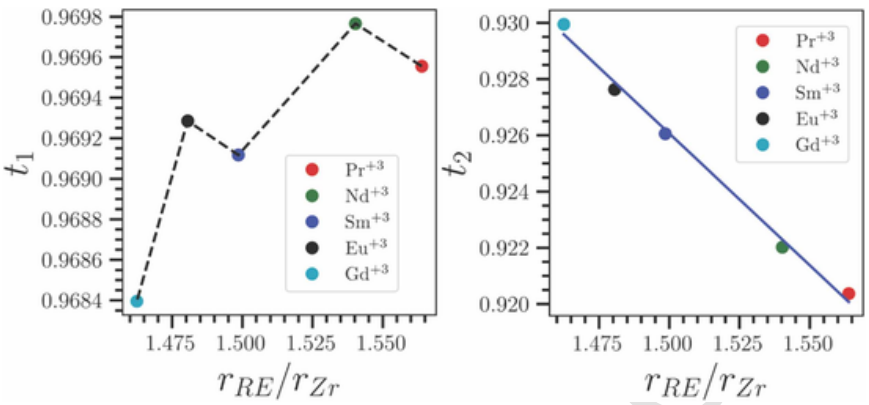

Fig. 5. : Relation between the tolerance factor t_1, and tolerance factor t_2 with the ratio (r_{RE}/r_{Zr}) of radii of RE and Zr species.

spect to the RE_4 tetrahedra with O' atom inside $RE_2Zr_2O_7$ unit (The tetrahedral environment around O and O' atoms is shown in Fig. 1, respectively). The tolerance factors t_1 and t_2 are found to be in the range 0.968–0.970 and 0.920–0.930, respectively. We found t_1 to be close to unity than t_2. Fig. 5 shows the variations of tolerance factors t_1 and t_2 with respect to radius ratio, r_{RE}/r_{Zr}. With a decrease in radius ratio r_{RE}/r_{Zr}, there is linear increase in the t_2.

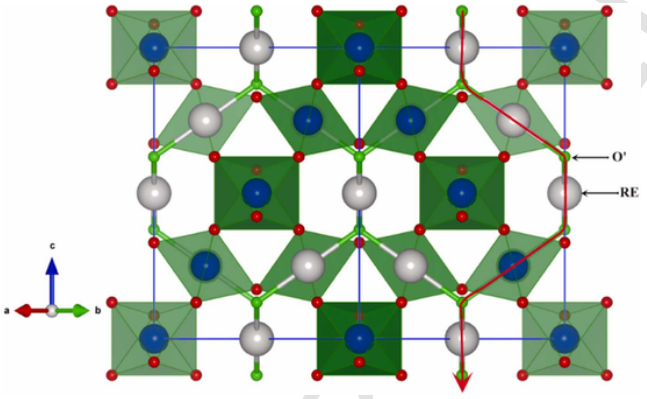

Fig. 6. : The connected O'-RE-O' network (part of which is shown by the red arrow) responsible for the dielectric screening (Color code: RE: gray, O': green, Zr: blue, and O: red).

3.3. Engineering the dielectric screening through the tolerance factors

The pyrochlore structure can be visualized as the framework of RE_2O' chains and ZrO_6 hexagonal units (see Fig. 6). The O'-RE-O' unit (contributing significantly to the dielectric screening due to the vibrational mode m_2) is a part of the RE_2O' network. This shows that the increase in the static dielectric constant is associated with the RE_2O' network of the pyrochlore zirconates. In fact, we can generalize that the enhancement of the static dielectric constants originates from the RE_2O'unit as shown in Fig. 6 in complex pyrochlores oxides.

Further, tolerance factor t_2 is defined with respect to the RE_4 tetrahedra with O' atoms at the center. This RE_4O' network is in fact a part of the RE_2O' chains in pyrochlore structure (see Fig. 6), indicating a direct relation of t_2 with the dielectric constant (see Fig. 7). Fig. 7 shows the variations of t_2 with $\Delta\varepsilon_2$ (due to O'-RE-O' bend) and the total static dielectric constant (ε_0) along the pyrochlore zirconate family.

Therefore, a direct one-to-one relationship of t_2 with ε_0 is established. Further this provides a handle to manipulate the dielectric response by a simple manipulation of t_2; the t_2 can be altered according to the Eq. (8). Specifically, the RE atom parameter in a material oxide can be modulated (e.g., by doping [55,56] the RE atom sites with an isovalent atomic species to find a desired dielectric response in variety of technological import pyrochlore oxides). Note that the temperature-induced changes in RE-O bond may alter the dielectric response which cannot be captured from the present DFT approach.

It may be noted that the classic way to determine the dielectric permittivity in molecular and solid systems is through the Clausius-Mossotti (C-M) relation [57] given by:

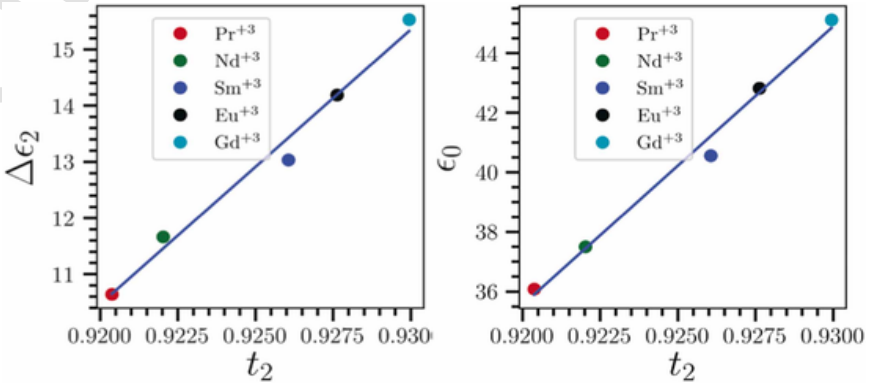

Fig. 7. : Relation between tolerance factor t_2 with a) the dielectric contribution of infrared active mode, $\Delta\varepsilon_2$, and b) with the static dielectric constants, ε_0, in pyrochlore zirconates.

$$\varepsilon_0 = (3V_m + 8\pi\alpha_D^m)/(3V_m - 4\pi\alpha_D^m)$$

where V_m and α_D^m are the volume and total polarizability of the molecular or solid system. To predict the ε_0, α_D^m is approximated from the individual polarizability of constituent units of the system. This has led to a good prediction for crystalline [58] materials although there is a limited database (from Shannon [59]) of individual dielectric polarizability of ionic species to make accurate ε_0 predictions from the C-M equation. Further, the underestimation of dielectric constant has been suggested in a study by Naoi *et al.* [60] Contrary to this, the present study employs DFT to estimate the ε_0 with electronic and phononic contributions leading to a better prediction of dielectric response. Further, relative importance of electronic and phononic parts to dielectric response is suggested using the present approach compared to the C-M relation.

4. Conclusions

The lattice vibrations of rare-earth pyrochlore zirconates, $RE_2Zr_2O_7$ (RE = Pr, Nd, Sm, Eu, and Gd) are explored using density functional theory. Out of the seven infrared active modes, three modes (m_2, m_3, and m_5) show a significant contribution towards the dielectric screening. Along the pyrochlore zirconate family, the dielectric constant increases due to the increase in its ionic part. This increase in the dielectric constant is due to the vibrational mode m_2 (O'-RE-O' bending which is part of RE_2O' chain in pyrochlore). In a nutshell, the RE_2O' unit is responsible for the dielectric screening in pyrochlore oxides.

Structurally, the environment around Zr^{4+} cations is found to be more like octahedron indicating that atomic arrangement is close to the ideal pyrochlore structure. However, along the pyrochlore zirconate family, there is an increase in the oxygen parameter leading to the fluorite structure. The tolerance factors t_1 and t_2 are calculated along with the variation of radius ratio (r_{RE}/r_{Zr}) for pyrochlore zirconates. With decrease in radius ratio, r_{RE}/r_{Zr}, a linear increase in tolerance factor t_2 is uncovered.

Variations of tolerance factors with the dominant ionic part of the static dielectric constant is studied, and a linear relation of t_2 with the dielectric constant along the pyrochlores zirconate family is established. The tolerance factor t_2 is associated to the RE_4 tetrahedra with O' atoms at the center. This tetrahedra is basically a part of the RE_2O' chains giving rise to significant dielectric response.

Author Statement

The author SK conceptualized, did calculations, investigated, and wrote the initial and reviewed the final manuscript. The KK and SN contributed to methodology part, reviewed and edited the final manuscript. The SK and RK reviewed and edited the final manuscript.

CRediT authorship contribution statement

Sonu Kumar: Writing – review & editing, Writing – original draft, Validation, Resources, Project administration, Methodology, Investigation, Formal analysis, Conceptualization. **Karan Deep:** Writing – review & editing, Methodology. **Shagun Nag:** Writing – review & editing, Methodology. **Ranjan Kumar:** Writing – review & editing.

Declaration of Competing Interest

The authors declare that they have no known competing financial interests or personal relationships that could have appeared to influence the work reported in this paper.

Data availability

Data will be made available on request.

Acknowledgments

SK gratefully acknowledges the partial financial support from the Council of Scientific and Industrial Research (CSIR) (reference: 09/086 (0946)/2009-EMR-I).

Appendix A. Supporting information

Supplementary data associated with this article can be found in the online version at doi:10.1016/j.mtcomm.2024.108415.

References

[1] L. Gao, K. Liang, Z. Guan, Z. Liu, Z. Fang, H. Chen, J. Zhang, Disordered structures and dielectric properties of Ni-doped bismuth magnesium niobate pyrochlores, J. Phys. Chem. C 125 (50) (2021) 27793–27799, https://doi.org/10.1021/acs.jpcc.1c08515.
[2] L. Gao, K. Liang, Z. Liu, H. Chen, J. Zhang, Structure dependence of dielectric properties in Ca-doped bismuth magnesium niobate pyrochlores, J. Alloy. Compd. 922 (2022) 165859, https://doi.org/10.1016/j.jallcom.2022.165859.
[3] M.-Y. Yan, L.-H. Shu, Y. Xing, L.-D. Chen, X.-Y. Zhang, S.-T. Zhang, Tailoring magnetic and dielectric properties of $Yb_2Ti_2O_7$ pyrochlore through structural distortion, Appl. Phys. Lett. 121 (26) (2022) 261901, https://doi.org/10.1063/5.0127341.
[4] S. Supriya, Influence of rare earth coordinated elements in titanium-based pyrochlores and their dielectric phenomena, Coord. Chem. Rev. 493 (2023) 215319, https://doi.org/10.1016/j.ccr.2023.215319.
[5] N.A. Zhuk, M.G. Krzhizhanovskaya, N.A. Sekushin, D.V. Sivkov, I.E. Abdurakhmanov, Crystal structure, dielectric and thermal properties of cobalt doped bismuth tantalate pyrochlore, J. Mater. Res. Technol. 22 (2023) 1791–1799, https://doi.org/10.1016/j.jmrt.2022.12.059.
[6] Y. Shimakawa, Y. Kubo, T. Manako, Giant magnetoresistance in Ti 2 Mn 2 O 7 with the pyrochlore structure, Nature 379 (6560) (1996) 53–55, https://doi.org/10.1038/379053a0.
[7] R. Vassen, X. Cao, F. Tietz, D. Basu, D. Stöver, Zirconates as new materials for thermal barrier coatings, J. Am. Ceram. Soc. 83 (8) (2000) 2023–2028, https://doi.org/10.1111/j.1151-2916.2000.tb01506.x.
[8] G.S.V. Coles, S.E. Bond, G. Williams, Metal stannates and their role as potential gas-sensing elements, J. Mater. Chem. 4 (1) (1994) 23–27, https://doi.org/10.1039/JM9940400023.
[9] S. Fujihara, K. Tokumo, Multiband orange-red luminescence of Eu3 + ions based on the pyrochlore-structured host crystal, Chem. Mater. 17 (22) (2005) 5587–5593, https://doi.org/10.1021/cm0513785.
[10] R.C. Ewing, W.J. Weber, J. Lian, Nuclear waste disposal—pyrochlore (A2B2O7): nuclear waste form for the immobilization of plutonium and "minor" actinides, J. Appl. Phys. 95 (11) (2004) 5949–5971, https://doi.org/10.1063/1.1707213.
[11] A. Chartier, C. Meis, J.-P. Crocombette, W.J. Weber, L.R. Corrales, Molecular dynamic simulation of disorder induced amorphization in pyrochlore, Phys. Rev. Lett. 94 (2) (2005) 025505, https://doi.org/10.1103/PhysRevLett.94.025505.
[12] W.J. Weber, R.C. Ewing, Plutonium immobilization and radiation effects, Science 289 (5487) (2000) 2051–2052, https://doi.org/10.1126/science.289.5487.2051.
[13] J.K. Gill, O.P. Pandey, K. Singh, Role of sintering temperature on thermal, electrical and structural properties of Y2Ti2O7 pyrochlores, Int. J. Hydrog. Energy 36 (22) (2011) 14943–14947, https://doi.org/10.1016/j.ijhydene.2011.02.138.
[14] C. Kinsler-Fedon, Q. Zheng, Q. Huang, E.S. Choi, J. Yan, H. Zhou, D. Mandrus, V. Keppens, Synthesis, Characterization, and single-crystal growth of a high-entropy rare-earth pyrochlore oxide, Phys. Rev. Mater. 4 (10) (2020) 104411, https://doi.org/10.1103/PhysRevMaterials.4.104411.
[15] M.A. Hubert, A.M. Patel, A. Gallo, Y. Liu, E. Valle, M. Ben-Naim, J. Sanchez, D. Sokaras, R. Sinclair, J.K. Nørskov, L.A. King, M. Bajdich, T.F. Jaramillo, Acidic oxygen evolution reaction activity–stability relationships in Ru-based pyrochlores, ACS Catal. 10 (20) (2020) 12182–12196, https://doi.org/10.1021/acscatal.0c02252.
[16] B. Santhosh Kumar, R.N. Perumal, C. Venkateswaran, Concurrence of ferroelectric, dielectric and magnetic behaviour in Tb2Ti2O7 pyrochlore, Phys. Lett. A 389 (2021) 127085, https://doi.org/10.1016/j.physleta.2020.127085.
[17] S.K. Sharma, H.S. Mohanty, D.K. Pradhan, A. Kumar, V.K. Shukla, F. Singh, P.K. Kulriya, Structural, Dielectric and electrical properties of pyrochlore-type Gd2Zr2O7 ceramic, J. Mater. Sci. Mater. Electron. 31 (24) (2020) 21959–21970, https://doi.org/10.1007/s10854-020-04699-4.
[18] J.W. Seo, J. Fompeyrine, A. Guiller, G. Norga, C. Marchiori, H. Siegwart, J.-P. Locquet, Interface formation and defect structures in epitaxial La2Zr2O7 thin films on (111) Si, Appl. Phys. Lett. 83 (25) (2003) 5211–5213, https://doi.org/10.1063/1.1635966.
[19] F. Wei, H. Tu, Y. Wang, S. Yue, J. Du, Epitaxial La2Hf2O7 Thin films on Si(001) substrates grown by pulsed laser deposition for high-k gate dielectrics, Appl. Phys. Lett. 92 (1) (2008) 012901, https://doi.org/10.1063/1.2828692.
[20] J.S. Gardner, M.J.P. Gingras, J.E. Greedan, Magnetic pyrochlore oxides, Rev. Mod. Phys. 82 (1) (2010) 53–107, https://doi.org/10.1103/RevModPhys.82.53.
[21] M.A. Subramanian, G. Aravamudan, G.V.S. Rao, Oxide pyrochlores - a review, Prog. Solid State Chem. 15 (1983) 55.
[22] A.F. Fuentes, K. Boulahya, M. Maczka, J. Hanuza, U. Amador, Synthesis of

disordered pyrochlores, A2Ti2O7 (A = Y, Gd and Dy), by mechanical milling of constituent oxides, Solid State Sci. 7 (4) (2005) 343–353, https://doi.org/10.1016/j.solidstatesciences.2005.01.002.
[23] M. Mączka, J. Hanuza, K. Hermanowicz, A.F. Fuentes, K. Matsuhira, Z. Hiroi, Temperature-dependent raman scattering studies of the geometrically frustrated pyrochlores Dy2Ti2O7, Gd2Ti2O7 and Er2Ti2O7, J. Raman Spectrosc. 39 (4) (2008) 537–544, https://doi.org/10.1002/jrs.1875.
[24] S. Kumar, H.C. Gupta, First principles study of zone centre phonons in rare-earth pyrochlore titanates, RE2Ti2O7 (RE = Gd, Dy, Ho, Er, Lu; Y), Vib. Spectrosc. 62 (2012) 180–187, https://doi.org/10.1016/j.vibspec.2012.06.001.
[25] S. Kumar, H.C. Gupta, First principles study of dielectric and vibrational properties of pyrochlore hafnates, Solid State Sci. 14 (10) (2012) 1405–1411, https://doi.org/10.1016/j.solidstatesciences.2012.08.003.
[26] M. Ruminy, M.N. Valdez, B. Wehinger, A. Bosak, D.T. Adroja, U. Stuhr, K. Iida, K. Kamazawa, E. Pomjakushina, D. Prabakharan, M.K. Haas, L. Bovo, D. Sheptyakov, A. Cervellino, R.J. Cava, M. Kenzelmann, N.A. Spaldin, T. Fennell, First-principles calculation and experimental investigation of lattice dynamics in the rare-earth pyrochlores R2Ti2O7 (R = Tb, Dy, Ho), Phys. Rev. B 93 (21) (2016) 214308, https://doi.org/10.1103/PhysRevB.93.214308.
[27] X. Gonze, C. Lee, Dynamical matrices, born effective charges, dielectric permittivity tensors, and interatomic force constants from density-functional perturbation theory, Phys. Rev. B 55 (16) (1997) 10355–10368, https://doi.org/10.1103/PhysRevB.55.10355.
[28] D. Fischer, A. Kersch, The Effect of Dopants on the dielectric constant of HfO2 and ZrO2 from first principles, Appl. Phys. Lett. 92 (1) (2008) 012908, https://doi.org/10.1063/1.2828696.
[29] A. Laturia, M.L.V. de Put, W.G. Vandenberghe, Dielectric properties of hexagonal boron nitride and transition metal dichalcogenides: from monolayer to bulk, Npj 2D Mater. Appl. 2 (1) (2018) 1–7, https://doi.org/10.1038/s41699-018-0050-x.
[30] J. Chun, P.G. Reuvekamp, D. Chen, C. Lin, R.K. Kremer, Promising high-k dielectric permittivity of pyrochlore-type crystals of Nd2Hf2O7, J. Mater. Chem. C 3 (3) (2014) 491–494, https://doi.org/10.1039/C4TC02416H.
[31] M.-Y. Yan, L.-H. Shu, Y. Xing, L.-D. Chen, X.-Y. Zhang, S.-T. Zhang, Tailoring magnetic and dielectric properties of Yb2Ti2O7 pyrochlore through structural distortion, Appl. Phys. Lett. 121 (26) (2022) 261901, https://doi.org/10.1063/5.0127341.
[32] V.M. Goldschmidt, Die Gesetze der Krystallochemie, Naturwissenschaften 14 (21) (1926) 477–485, https://doi.org/10.1007/BF01507527.
[33] D.Y. Suárez, I.M. Reaney, W.E. Lee, Relation between tolerance factor and Tc in aurivillius compounds, J. Mater. Res. 16 (11) (2001) 3139–3149, https://doi.org/10.1557/JMR.2001.0433.
[34] L. Cai, A.L. Arias, J.C. Nino, The tolerance factors of the pyrochlore crystal structure, J. Mater. Chem. 21 (11) (2011) 3611–3618, https://doi.org/10.1039/C0JM03380D.
[35] S. Baroni, S. de Gironcoli, A. Dal Corso, P. Giannozzi, Phonons and related crystal properties from density-functional perturbation theory, Rev. Mod. Phys. 73 (2) (2001) 515–562, https://doi.org/10.1103/RevModPhys.73.515.
[36] D. Vanderbilt, Soft self-consistent pseudopotentials in a generalized Eigenvalue formalism, Phys. Rev. B 41 (11) (1990) 7892–7895, https://doi.org/10.1103/PhysRevB.41.7892.
[37] P. Giannozzi, S. Baroni, N. Bonini, M. Calandra, R. Car, C. Cavazzoni, Ceresoli Davide, G.L. Chiarotti, M. Cococcioni, I. Dabo, A.D. Corso, S. de Gironcoli, S. Fabris, G. Fratesi, R. Gebauer, U. Gerstmann, C. Gougoussis, Kokalj Anton, M. Lazzeri, L. Martin-Samos, N. Marzari, F. Mauri, R. Mazzarello, Paolini Stefano, A. Pasquarello, L. Paulatto, C. Sbraccia, S. Scandolo, G. Sclauzero, A.P. Seitsonen, A. Smogunov, P. Umari, R.M. Wentzcovitch, QUANTUM ESPRESSO: a modular and open-source software project for quantum simulations of materials, J. Phys. Condens. Matter 21 (39) (2009) 395502, https://doi.org/10.1088/0953-8984/21/39/395502.
[38] J.P. Perdew, A. Zunger, Self-interaction correction to density-functional approximations for many-electron systems, Phys. Rev. B 23 (10) (1981) 5048–5079, https://doi.org/10.1103/PhysRevB.23.5048.
[39] D.M. Ceperley, B.J. Alder, Ground state of the electron gas by a stochastic method, Phys. Rev. Lett. 45 (7) (1980) 566–569, https://doi.org/10.1103/PhysRevLett.45.566.
[40] J.P. Perdew, K. Burke, M. Ernzerhof, Generalized gradient approximation made simple, Phys. Rev. Lett. 77 (18) (1996) 3865–3868, https://doi.org/10.1103/PhysRevLett.77.3865.
[41] J.P. Perdew, A. Ruzsinszky, G.I. Csonka, O.A. Vydrov, G.E. Scuseria, L.A. Constantin, X. Zhou, K. Burke, Restoring the density-gradient expansion for exchange in solids and surfaces, Phys. Rev. Lett. 100 (13) (2008) 136406, https://doi.org/10.1103/PhysRevLett.100.136406.
[42] J.M. Pruneda, E. Artacho, First-principles study of structural, elastic, and bonding properties of pyrochlores, Phys. Rev. B 72 (8) (2005) 085107, https://doi.org/10.1103/PhysRevB.72.085107.
[43] Karandeep, H.C. Gupta, S. Kumar, First principles study of structural and vibrational properties of Ba2YTaO6 in Cubic and Tetragonal Phases, J. Alloy. Compd. 555 (Supplement C) (2013) 335–338, https://doi.org/10.1016/j.jallcom.2012.12.086.
[44] S. Kumar, H.C. Gupta, Karandeep, First principles study of structural, bonding and vibrational properties of PtCoO2, PdCoO2 and PdRhO2 metallic delafossites, J. Phys. Chem. Solids 74 (2) (2013) 305–310, https://doi.org/10.1016/j.jpcs.2012.10.004.
[45] Kumar, S. Electronic Structure Automater (EStA). ⟨https://skphy.github.io/esta/html/index.html⟩ (accessed 2023-04-16).
[46] R. Fletcher, Practical Methods of Optimization, second ed., Wiley: A Wiley-Interscience publication, Chichester, 2008.
[47] H.J. Monkhorst, J.D. Pack, Special points for brillouin-zone integrations, Phys. Rev. B 13 (12) (1976) 5188–5192, https://doi.org/10.1103/PhysRevB.13.5188.
[48] A. Togo, L. Chaput, T. Tadano, I. Tanaka, Implementation strategies in phonopy and phono3py, J. Phys. Condens. Matter 35 (35) (2023) 353001, https://doi.org/10.1088/1361-648X/acd831.
[49] A. Togo, First-principles phonon calculations with phonopy and phono3py, J. Phys. Soc. Jpn. 92 (1) (2023) 012001, https://doi.org/10.7566/JPSJ.92.012001.
[50] W.G. Fateley, N.T. McDevitt, F.F. Bentley, Infrared and Raman selection rules for lattice vibrations: the correlation method, Appl. Spectrosc. 25 (2) (1971) 155–173.
[51] R.A. McCauley, Infrared-absorption characteristics of the pyrochlore structure, ⁎. JOSA 63 (6) (1973) 721–725, https://doi.org/10.1364/JOSA.63.000721.
[52] R.A. McCauley, Structural characteristics of pyrochlore formation, J. Appl. Phys. 51 (1) (1980) 290–294, https://doi.org/10.1063/1.327368.
[53] B.J. Kennedy, Structural trends in pyrochlore-type oxides, Phys. B Condens. Matter 241–243 (1997) 303–310, https://doi.org/10.1016/S0921-4526(97)00570-X.
[54] K.E. Sickafus, R.W. Grimes, J.A. Valdez, A. Cleave, M. Tang, M. Ishimaru, S.M. Corish, C.R. Stanek, B.P. Uberuaga, Radiation-induced amorphization resistance and radiation tolerance in structurally related oxides, Nat. Mater. 6 (3) (2007) 217–223, https://doi.org/10.1038/nmat1842.
[55] Z. Qu, C. Wan, W. Pan, Thermal expansion and defect chemistry of MgO-Doped $Sm_2Zr_2O_7$, Chem. Mater. 19 (20) (2007) 4913–4918, https://doi.org/10.1021/cm071615z.
[56] D. Zhang, C. Yang, D. Liu, Y. Liu, P. Zhou, L. Ren, D. Sun, Achieving the synergy of low thermal conductivity and superior mechanical properties of Ce Doping La2Zr2O7 ceramics for thermal protection coatings: experiment and first-principles calculations, J. Phys. Chem. Solids 163 (2022) 110606, https://doi.org/10.1016/j.jpcs.2022.110606.
[57] J.G. Kirkwood, On the theory of dielectric polarization, J. Chem. Phys. 4 (9) (1936) 592–601, https://doi.org/10.1063/1.1749911.
[58] J.I. Viegas, S. Thomas, R.N. Gontijo, A. Righi, R.L. Moreira, A. Dias, Vibrational spectroscopy and intrinsic dielectric properties of Sr2RE8(SiO4)6O2 (RE = Rare Earth) ceramics, Mater. Res. Bull. 146 (2022) 111616, https://doi.org/10.1016/j.materresbull.2021.111616.
[59] R.D. Shannon, Dielectric polarizabilities of ions in oxides and fluorides, J. Appl. Phys. 73 (1) (1993) 348–366, https://doi.org/10.1063/1.353856.
[60] T.A. Naoi, R.B. Van Dover, Dielectric properties of amorphous Ta-Ge-O and Ta-Si-O thin films, J. Appl. Phys. 123 (24) (2018) 244103, https://doi.org/10.1063/1.5022336.